FACILE SYNTHESIS OF FUNCTIONALIZED UiO-66-TYPE MOFs FOR CO$_2$ ADSORPTION

Article

Jinlong Ge[a,b,*,], Xiaoqi Jin[a,b], Liyuan Zhang[a,b], Yuhong Jiao[a,b], Qiuqin Wang[a,b], Yongkui Wang[a,b], Yan Gao[a,b], Jiaojiao Geng[a,b] and Tianqi Wang[a,b]

[a]School of Materials and Chemical Engineering, Bengbu University, 233030 Bengbu, Anhui, China
[b]Anhui Provincial Engineering Laboratory of Silicon-based Materials, 233030 Bengbu, Anhui, China

The metal-organic frameworks (MOFs) UiO-66-NH$_2$, UiO-66-2,5-(OH)$_2$, UiO-66-NO$_2$, UiO-66-NDC, and UiO-66-BPDC were synthesized under solvothermal conditions using different functionalized organic linkers. The structures and properties of the samples were characterized by X-ray diffraction, Fourier transform infrared spectroscopy, thermogravimetric analysis, scanning electron microscopy, and nitrogen adsorption-desorption isotherms. The crystal structures of these functionalized UiO-66(Zr) forms were similar. A series of functionalized UiO-66(Zr) samples were used in the adsorption of carbon dioxide (CO$_2$). UiO-66-NH$_2$ had the highest CO$_2$ adsorption capacity (about 3.35 mmol g^{-1}) due to its small polar –NH$_2$ group. The performance of UiO-66-NH$_2$ in CO$_2$ adsorption at different temperatures was also determined. The amino-functionalized material possessed better adsorption properties at 273 K than at 303 K, while the CO$_2$ working capacity of UiO-66-NH$_2$ was fully recovered after cyclic regeneration.

Keywords: metal-organic frameworks; CO$_2$ adsorption; UiO-66-type MOFs; UiO-66-NH$_2$; functionalized linker.

INTRODUCTION

Metal-organic frameworks (MOFs) are a versatile class of crystalline and porous materials made up of metal clusters or metal ions bound to organic ligands by coordination bonds.[1,2] These hybrid materials have extremely high specific surface areas and active pore volumes,[3] uniform pore sizes,[4] and chemical functionalities.[5] Owing to their unique features, MOFs have attracted considerable attention for their possible application in gas storage,[6] catalysis,[7] separation,[8] drug delivery,[9] and sensors. Today, the rising level of carbon dioxide (CO$_2$) in the atmosphere has led to drastic changes in the climate and ecosystem that pose a potential threat to human health and life.[10] Thus, CO$_2$ capture from industry sectors or directly from the atmosphere has drawn significant attention on a global scale.[11,12] Reducing CO$_2$ emissions from burning processes *via* capture and storage has been proposed as a potential control strategy, which has been extensively studied using different methods.[13] Conventional CO$_2$ capture using porous media has been considered an efficient alternative to amine-based chemisorption.[14,15] However, amine-functionalized porous materials have superior CO$_2$ adsorption capacity and regeneration efficiency,[16] leading to extensive efforts focusing on enhancing the gas separation properties, selectivity, and permeability of alternative approaches.[17]

MOFs have advantages over conventional adsorbents for mixture separation because of their gas storage and separation properties,[18] catalytic performance, and host-guest exchange mechanism.[19] Numerous MOF structures have been developed with great gas separation performance. As efficient CO$_2$ adsorbers, these MOFs have specific characteristics and requirements such as high porosity, good thermal stability, organic nitrogen-containing heterocyclic ligands, functional groups, and open metal sites.[20]

UiO-66 [Zr$_6$O$_4$(OH)$_4$(O$_2$CC$_6$H$_4$CO$_2$)$_6$] is composed of Zr$_6$O$_4$(OH)$_4$ clusters linked to 12 terephthalate ligands, which are interconnected by triangular windows (d = 6 Å).[21] UiO-66 has attracted much

attention in CO$_2$/CH$_4$ gas separation due to its good selectivity, high working capacity, and low-cost regeneration ability.[22] The remarkable stability of this solid was well suited for further investigation into its functionalization effect on CO$_2$ capture. In addition, polar functional groups can be grafted onto MOFs to design more efficient CO$_2$ capture materials.

Several polar functional groups (*e.g.*, –NH$_2$, –NO$_2$, –OH, –(CF$_3$)$_2$, –SO$_3$H, and –CO$_2$H) have been used to prepare functionalized MOFs to enhance the uptake of CO$_2$ and CH$_4$.[23] The functionalized samples displayed higher CO$_2$ adsorption, good working capacities, and moderate CO$_2$ adsorption enthalpy values. Specifically, amino-functionalized UiO-66 with high polarity and small functional group size possessed the best adsorption properties,[24] while naphthyl-functionalized UiO-66 exhibited inhibited water vapor adsorption and high CO$_2$ selectivity.[25]

In this work, UiO-66-NH$_2$, UiO-66-2,5-(OH), UiO-66-NO$_2$, UiO-66-NDC, and UiO-66-BPDC were synthesized with different functional groups. By varying the inorganic or organic building unit, their modular build-up offered unprecedented flexibility in structural fine-tuning. The samples were characterized and their textural properties and CO$_2$ adsorption ability were compared with singly functionalized MOFs. The materials demonstrated excellent modulation in internal structure, particle morphology, and outer surface functionalities with high porosity, excellent stability, and high CO$_2$ adsorption performance.

EXPERIMENTAL

Materials

Zirconium(IV) chloride, *N,N*-dimethylformamide (DMF), ethanol, 2-aminoterephthalic acid (98%) (BDC-NH$_2$), 2,5-dihydroxybenzene dicarboxylic acid (BDC-(OH)$_2$), 2-nitroterephthalic acid (BDC-NO$_2$, ≥ 99%), 1,4-naphthalenedicarboxylic acid (NDC), 4,4'-biphenyl-dicarboxylate (BPDC) were purchased from Sinopharm Chemical Reagent Co., Ltd (China). All chemicals were used as received without further purification.

*e-mail: jinlongge2005@126.com

Preparation of MOFs

The synthesis of NH_2-UiO-66 was based on a previously reported procedure.[26] The standard upscaled synthesis of NH_2-UiO-66 was performed by dissolving $ZrCl_4$ (1.50 g, 6.4 mmol) and 2-aminoterephthalic acid (1.56 g, 6.4 mmol) in *N*-dimethylformamide (DMF) (180 mL) at room temperature in a volumetric flask. The resulting mixture was placed in a preheated oven at 80 °C for 12 h and then held at 100 °C for 24 h. After the solution was cooled to room temperature in air, the resulting solid was filtered and repeatedly washed with absolute ethanol for 3 days while being heated at 60 °C in a water bath. The resulting yellow powder was filtered and dried under vacuum at 60 °C. UiO-66-2,5-$(OH)_2$, UiO-66-NO_2, UiO-66-NDC, and UiO-66-BPDC were synthesized analogously by replacing BDC-NH_3 with the equivalent molar amounts of BDC-$(OH)_2$, BDC-NO_2, NDC, and BPDC, respectively. The different chemical structures of the functionalized BDC linkers are shown in Figure 1. The functionalized ligands independently contributed to the modified chemical and physical properties of UiO-66.
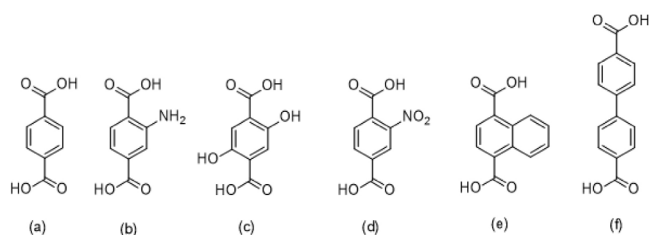
Figure 1. The chemical structure of linkers used for synthesizing UiO-66-type MOFs: (a) BDC, (b) BDC-NH_2, (c) BDC-$(OH)_2$, (d) BDC-NO_2, (e) NDC and (f) BPDC

Characterization

The crystal structures of the samples were characterized by powder X-ray diffraction (XRD) on a Rigaku SmartLab SE (Rigaku, Japan) with Cu Kα radiation (λ = 1.54056 Å). The diffraction data were collected over the angular range of 3-40° with a step size of 0.02° at 35 kV and 20 mA. Fourier transform infrared (FT-IR) spectra were measured using KBr pellets on a Nicolet iS10 analyzer (Thermo Scientific Nicolet, USA) in the spectral range of 4000-400 cm^{-1} with 4 cm^{-1} resolution. The samples were treated using the potassium bromide pellet technique before testing. Thermogravimetric analysis (TGA) was performed on STA 2500 Regulus analyzer (Netzsch, Germany) in the temperature range of 30-900 °C at a heating rate of 10 °C min^{-1} under nitrogen flow. Nitrogen adsorption-desorption isotherms were obtained at 77 K using a Micromeritics ASAP 3020 Sorptometer (Micromeritics Instrument Corporation, USA). The surface area based on N_2 isotherm data was analyzed by Brunauer-Emmett-Teller (BET). The structure and morphology of the samples were investigated using Zeiss Sigma 300 scanning electron microscope (Germany) at an acceleration voltage of 15 kVA.

Gas sorption measurements

The CO_2 sorption isotherms of UiO-66-type MOFs were measured using a Micromeritics ASAP 3020 surface area and pore size analyzer (Thermo Scientific Nicolet, USA). High-purity CO_2 was used for gas sorption measurements, and the samples had been degassed at 150 °C for 10 h beforehand. The temperature of the samples was maintained at 273 K using an ice water bath and controlled at 293 and 303 K by circulating water. The CO_2 adsorption capacities were calculated using the volumetric method.

RESULTS AND DISCUSSIONS

X-ray diffraction (XRD) measurements

The XRD patterns of the UiO-66(Zr)-type MOFs are displayed in Figure 2. The MOF samples with different functional groups exhibited high degrees of crystallinity, which were in good agreement with that previously reported in the parent UiO-66 MOF. The structures of the zirconium(IV)-based MOFs were built from $Zr_6O_4(OH)_4$ oxo clusters bound to twelve terephthalate (BDC) ligands.[27] The inorganic brick of the $Zr_6O_4(OH)_4$ core and the triangular faces of the Zr_6 octahedron were alternatively capped by μ3-O and μ3-OH groups.[28] The XRD patterns for UiO-66-NH_2, UiO-66-2,5-$(OH)_2$, and UiO-66-NO_2 presented sharper and narrower diffraction peaks at 2θ = 7.3, 8.5, 17.1, 25.8, and 30.8°. The two peaks at 7.3 and 8.5° respectively represented the (111) and (200) crystal planes. For UiO-66-NDC and UiO-66-BPDC, the diffraction peaks shifted slightly from 7.3 to 6°.[29] The longer NDC and BPDC organic linkers of UiO-66-NDC and UiO-66-BPDC led to an expanded pore size and ordered crystal defects compared to the shorter organic linkers of UiO-66-NH_2, UiO-66-2,5-$(OH)_2$, and UiO-66-NO_2. The inorganic brick in the structure was still a 12-coordinated $Zr_6O_4(OH)_4(CO_2)_{12}$ cluster,[28] but the defects in the MOFs may generate additional exposed metal sites that can serve as Lewis acids in gas adsorption.[30] The functional groups on the rotational motions of the organic linker also affected the pore size and adsorption of CO_2.
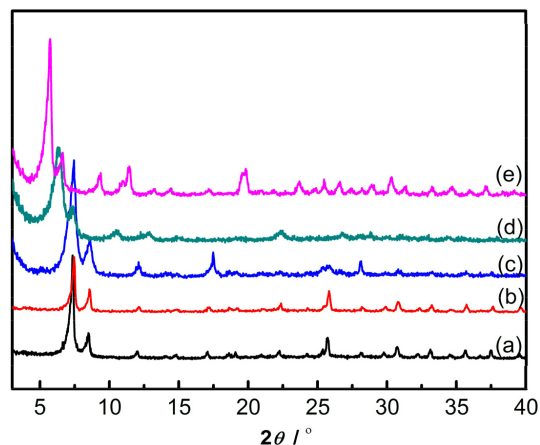
Figure 2. XRD patterns of as-synthesized UiO-66 MOFs: (a) UiO-66-NH_2, (b) UiO-66-2,5-$(OH)_2$, (c) UiO-66-NO_2, (d) UiO-66-NDC and (e) UiO-66-BPDC

Fourier transform infrared (FTIR) measurements

The FTIR spectra of these functionalized UiO-66-type MOFs are shown in Figure 3. Similar characteristic peaks were observed for all synthesized MOF particles. The hydroxyl peak for the UiO-66-NH_2, UiO-66-2,5-$(OH)_2$, UiO-66-NO_2, UiO-66-NDC, and UiO-66-BPDC samples was observed at 3300.10 cm^{-1}. The two intense bands near 1572.15 and 1387.73 cm^{-1} were respectively attributed to C–O asymmetric and symmetric stretching vibrations in the carboxylate group of UiO-66-NH_2BDC and UiO-66-2,5-$(OH)_2$.[31] The small band around 1497.35 cm^{-1} represented C–C vibrations in the benzene ring of the different functionalized linkers. For the UiO-66-NO_2 sample, the absorption band at 1361.25 cm^{-1} can be attributed to the C–N symmetric stretching of the nitro functional group in the aromatic carboxylate salt.[32] The C–N stretching vibration peak near 870 cm^{-1} usually present in nitroaromatic compounds could not be easily observed. Additional peaks between 664.89 and 964.80 cm^{-1} were ascribed to the bending and twisting of the Zr node and the C–Br bond

vibration.[33] The peaks at 483.20 and 582.96 cm⁻¹ were assigned to the Zr–O stretching mode. Although there are no pure C–X stretching vibrational modes for aromatic halogen compounds, it is difficult to assign Zr and functionalized linkers to a specific stretching mode. However, nitro and other functional groups were evidenced by the relatively low concentration of formed functionalized groups between the UiO-66-type particles.[34]
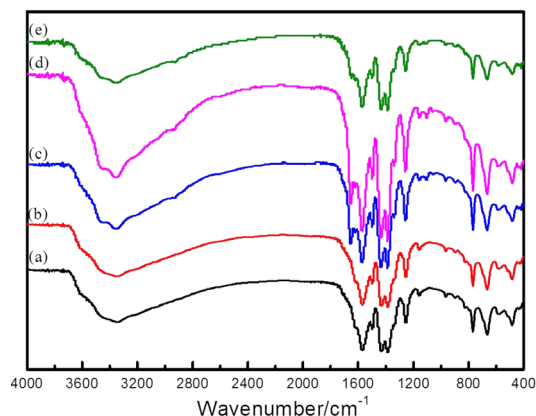
Figure 3. *FTIR spectra of as-synthesized UiO-66 MOFs: (a) UiO-66-NH₂, (b) UiO-66-2,5-(OH)₂, (c) UiO-66-NO₂, (d) UiO-66-NDC and (e) UiO-66-BPDC*

Thermogravimetric (TG) measurements

All of the TG analyses were carried out in N_2 to investigate the thermal stability of the samples. Over a temperature range of 35-100 °C, all samples exhibited the loss of physisorbed water molecules and solvent molecules hosted in the pores (Figure 4).[35] The as-synthesized samples showed an initial weight loss of 8%, with progressive weight loss at 200-350 °C corresponding to the removal of monocarboxylate ligands and the dehydroxylation of the six Zr cornerstones. The UiO-66-2,5-(OH)₂ structure started to decompose around 210 °C, while UiO-66-NO₂ remained thermally stable until 400 °C. These findings are supported by the polarity of the hydroxyl groups, which was higher than that of the NO₂ groups. The thermogravimetric analyses of UiO-66-NDC and UiO-66-BPDC were characterized by a mass loss between 500 and 600 °C attributable to linker volatilization. After 400 °C, the functional groups of the coordinated organic linkers inside the pores were broken and the structures collapsed. In all, the functionalized UiO-66-type MOFs exhibited high thermal stabilities up to 400 °C suitable for high-temperature applications.[36]
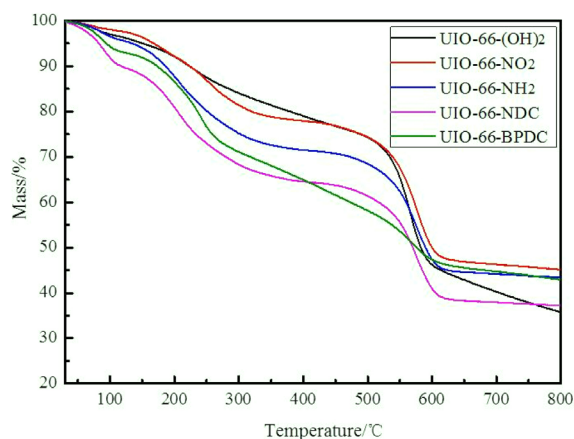
Figure 4. *Thermogravimetric analysis (TGA) curves of as-synthesized UiO-66 MOFs*

Brunauer-Emmett-Teller (BET) measurements

The N_2 adsorption-desorption isotherms were collected and are shown in Figure 5. The isotherms of the crystalline MOF samples retained their porosity despite the presence of different functional groups on the linker.[37] The specific BET surface area of NH₂-UiO-66 was 1556 m² g⁻¹, while that of bare UiO-66 was 1320 m² g⁻¹. The BET surface areas for different linkers, UiO-66-NO₂, UiO-66-2,5-(OH)₂, UiO-66-NDC, and UiO-66-BPDC, were calculated as 825, 765, 485, and 397 m² g⁻¹, respectively. The electronic and steric effects of the large and heavy functional groups reduced the free space available and largely decreased the porosity.[38]
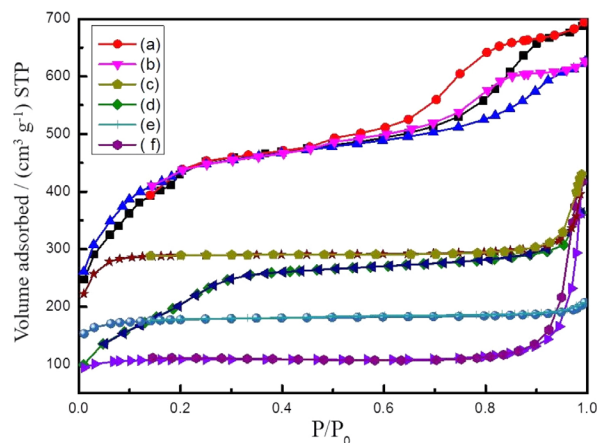
Figure 5. *N_2 adsorption-desorption isotherms of as-synthesized UiO-66 MOFs: (a) UiO-66-NH₂, (b) UiO-66-2,5-(OH)₂, (c) UiO-66-NO₂, (d) UiO-66, (e) UiO-66-NDC and (f) UiO-66-BPDC*

The pore sizes of the functionalized UiO-66-type MOFs are shown in Table 1 and Figure 6. The internal pores of the functionalized UiO-66-type MOFs were limited by the triangular windows of 6 Å, which corresponded with the crystal model. However, their pore sizes decreased from 6 to 4 Å, which can be attributed to the vacancy defects provided by the functionalized groups.[39] These samples remain highly microporous and with an average pore size of about 2.1 nm.[40] Furthermore, the reduced specific surface area and micropore volume indicated the partial collapse of the local pore structure due to the different functionalized linkers.[41] Such a small pore size can provide highly favorable van der Waals interactions that are conducive to CO_2 adsorption.

Scanning electron microscopy (SEM) measurements

The SEM images of all the samples are shown in Figure 7. As illustrated in Figure 7, the morphology of UiO-66 and UiO-66-NH₂ samples were exhibited perfectly uniform octahedral morphologies. UiO-66-2,5-(OH)₂ and UiO-66-NO₂ particles were determined to be a triangular-base pyramid shape with a size of about 250-400 nm.[42] UiO-66-NDC and UiO-66-BPDC were identified to be small and irregular typical octahedral morphology with a crystal size of about 150 nm, which is smaller than that of UiO-66-2,5-(OH)₂ and UiO-66-NO₂.[20] These results suggest that the functional groups did not significantly affect the crystal size.[43]

CO_2 adsorption

MOFs containing polar functional groups exhibited stronger interactions with CO_2 and have demonstrated great potential for CO_2 capture. The ideal adsorbents for this operation should

Table 1. Surface area and pore volumes of as-synthesized UiO-66 MOFs

Number	UiO-MOFs	BET / $(m^2\ g^{-1})$	Langmuir / $(m^2\ g^{-1})$	Pore volume / $(cm^3\ g^{-1})$
1	UiO-66-NH$_2$	1556	2156	2.7
2	UiO-66	1320	1453	2.4
3	UiO-66-NO$_2$	825	896	2.3
4	UiO-66-2,5-(OH)$_2$	765	793	4.0
5	UiO-66-NDC	485	512	2.1
6	UiO-66-BPDC	397	463	2.1

have high working capacity, good selectivity, and excellent stability.[31]

The CO$_2$ adsorption isotherms of UiO-66, UiO-66-NH$_2$, UiO-66-2,5-(OH)$_2$, UiO-66-NO$_2$, UiO-66-NDC, and UiO-66-BPDC were evident within the measured range of pressures at 273 K (Figure 8). Specifically, UiO-66-NH$_2$ with the small, polar –NH$_2$ group achieved the best performance, providing a higher CO$_2$ adsorption capacity (about 3.35 mmol g^{-1}) than that with the other bulkier groups.[44]

The CO$_2$ adsorption capacity of the UiO-66-NO$_2$ sample was higher than that of UiO-66-(OH)$_2$ but lower than that of UiO-66-NH$_2$. CO$_2$ strongly interacts with polar functional groups. The higher polarity of the –NO$_2$ organic linker led to strong dipole-dipole dispersion interactions that indirectly enhanced CO$_2$ adsorption.[45]

Interestingly, the CO$_2$ equilibrium adsorption capacity of UiO-66 was lower than that of UiO-66-NO$_2$ due to the nonpolar organic linkers. The CO$_2$ working capacity was further calculated to be 1.30 mmol g^{-1} for the parent UiO-66 molecule. Entry to the internal

pores of UiO-66 was limited by the 6 Å triangular windows, as the effect of pore volume becomes more important and favorable adsorption sites are not occupied without the functional group.[35]

The adsorption capacity of UiO-66-2,5-(OH)$_2$ was slightly lower than that of UiO-66-NO$_2$, due to the strong chemical bonding between the functional OH groups of the organic linkers and the metal cores, which have higher polarity and greater affinity toward CO$_2$. The synergistic effect of the Brønsted acid sites and the small pore size of UiO-66-2,5-(OH)$_2$ may have also boosted its CO$_2$ uptake capacity.[46]

UiO-66-BPDC and UiO-66-NDC exhibited CO$_2$ uptake values of 0.55 and 0.73 mmol g^{-1}, respectively, which were lower than the CO$_2$ uptake values of the other polar functional groups.[15] The introduction of naphthyl bidentate functional groups imparted a greater molar mass, lower pore volume, and steric hindrance near the metal cluster without significantly strengthening the surface binding sites, thus leading to decreased adsorption performance at higher CO$_2$ loadings.[47] The low working capacities of UiO-66-NDC and UiO-66-BPDC likely resulted from their limited surface areas. The lower BET surface area influenced the direct adsorption between functional groups and the CO$_2$ molecule.[14] Thus, the increase in the adsorption enthalpy of CO$_2$ in the modified materials generally corresponded to the polarity for the functional group: –BPDC < –NDC < –OH < –NO$_2$ < –NH$_2$.[48] The enhanced CO$_2$ affinity of the MOF seemed to relate to the intrinsic properties of the functional group. The CO$_2$ adsorption capacities of the UiO-66-type MOFs at 273 K are shown in Table 2.

The CO$_2$ adsorption isotherms of NH$_2$-UiO-66 are shown in Figure 9. The CO$_2$ uptake values of NH$_2$-UiO-66 were 1.70, 1.56, and 1.13 mmol g^{-1} at 273, 293, and 303 K, respectively. The CO$_2$ working capacity at 273 K was 33% lower than that at 303 K. The decrease in isosteric heat of adsorption with CO$_2$ gas loading resulted from the
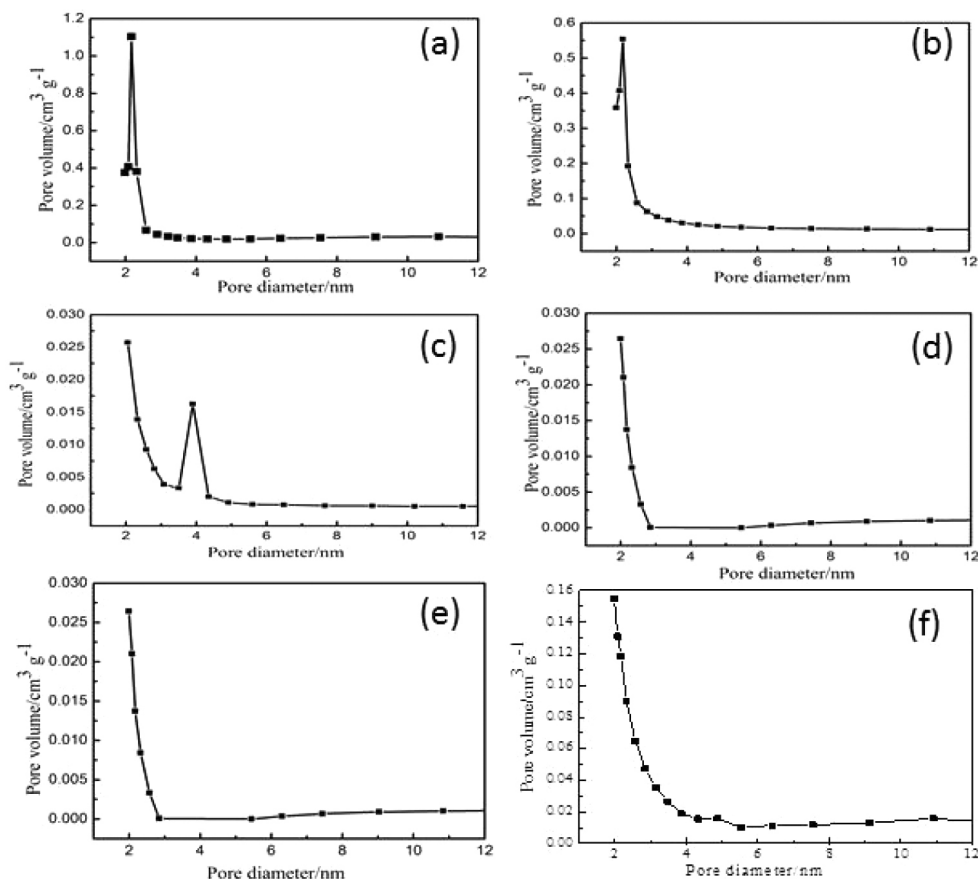
Figure 6. *Pore diameter of as-synthesized UiO-66 MOFs: (a) UiO-66-NH$_2$, (b) UiO-66-2,5-(OH)$_2$, (c) UiO-66-NO$_2$, (d) UiO-66-NDC, (e) UiO-66-BPDC and (f) UiO-66*
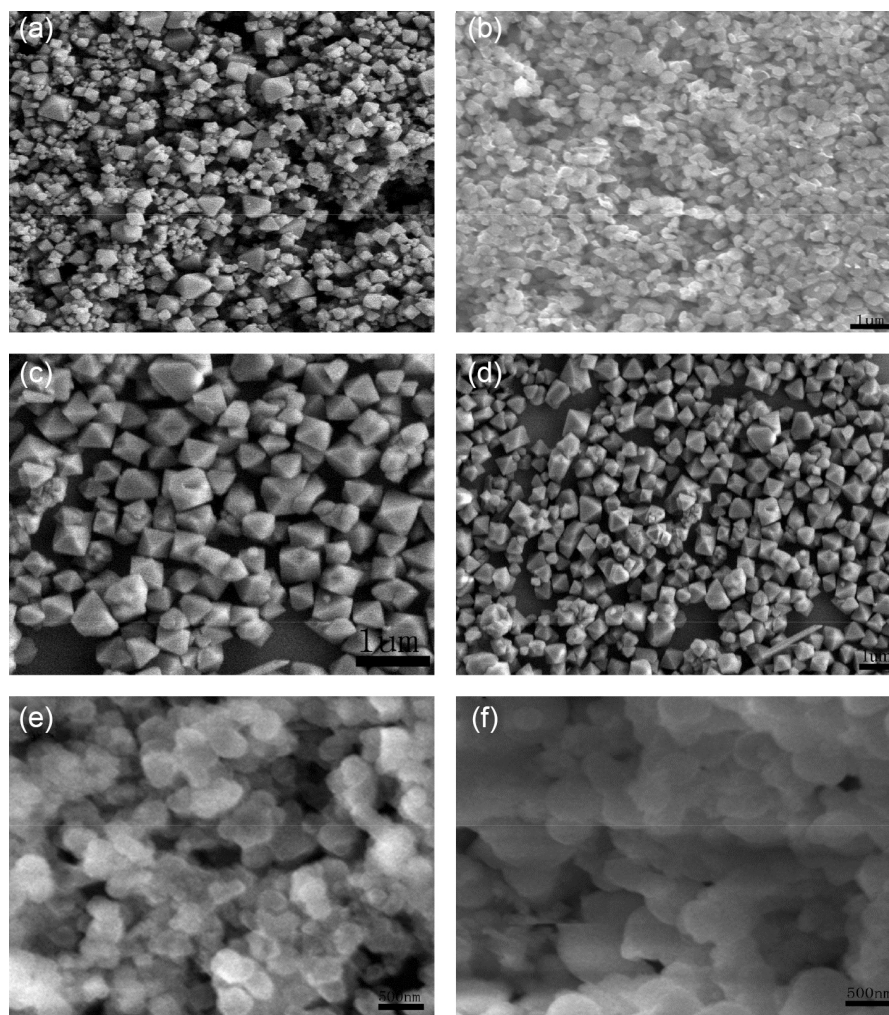
Figure 7. SEM of as-synthesized UiO-66 MOFs: (a) UiO-66, (b) UiO-66-NH₂, (c) UiO-66-2,5-(OH)₂, (d) UiO-66-NO₂, (e) UiO-66-NDC and (f) UiO-66-BPDC
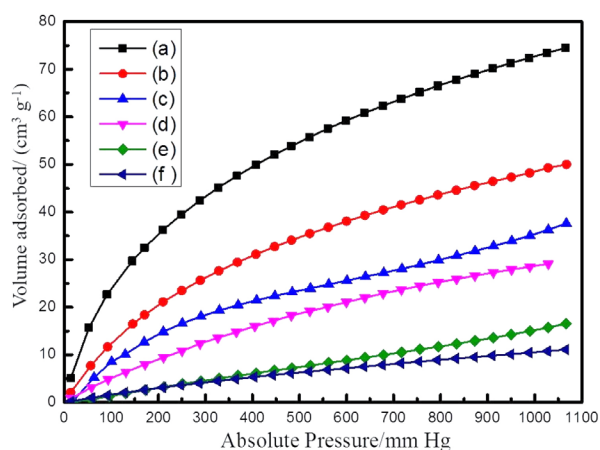
Figure 8. CO_2 adsorption isotherm of as-synthesized UiO-66 MOFs at 273 K: (a) UiO-66-NH₂, (b) UiO-66-2,5-(OH)₂, (c) UiO-66-NO₂, (d) UiO-66, (e) UiO-66-NDC and (f) UiO-66-BPDC

Table 2. CO_2 adsorption capacity of as-synthesized UiO-66 MOFs at 273 K

Number	Materials	CO_2 uptake / (mmol g^{-1})
1	UiO-66-NH₂	3.35
2	UiO-66	1.27
3	UiO-66-NO₂	1.72
4	UiO-66-2,5(OH)₂	2.2
5	UiO-2,6-NDC	0.73
6	UiO-66-BPDC	0.55

has a relatively flat isosteric heat adsorption profile, which is desirable for efficient adsorbent regeneration. The stability and robustness of UiO-66-NH₂ were investigated by recovering the solid after five consecutive adsorption cycles (Figure 10). The respective CO_2 uptake values of NH₂-UiO-66 after each cycle were 1.70, 1.66, 1.25, 1.22, and 1.09 mmol g^{-1}, demonstrating the reversibility of the CO_2 adsorption-desorption process for NH₂-UiO-66.[49] This phenomenon was mainly attributed to the –NH₂ groups from the functional ligands, which increased the interactions between CO_2 molecules and the host framework.

CONCLUSIONS

In summary, we successfully synthesized a series of UiO-66-type MOFs (*i.e.*, UiO-66-NH₂, UiO-66-2,5-(OH)₂, UiO-66-NO₂,

high heterogeneity of the adsorbents with a wide distribution of gas-solid interaction energies.[49] The higher CO_2 sorption capacity at 273 K was attributed to the reduced kinetic barrier at lower temperatures, which corresponded to the facilitated CO_2 desorption from the NH₂-UiO-66 surface at higher temperatures.[50]

Adsorbent regeneration is an important parameter used to evaluate the feasibility of the adsorbent for industrial applications. UiO-66-NH₂

Figure 9. *CO₂ adsorption isotherm of UiO-66-NH₂ at different temperature*
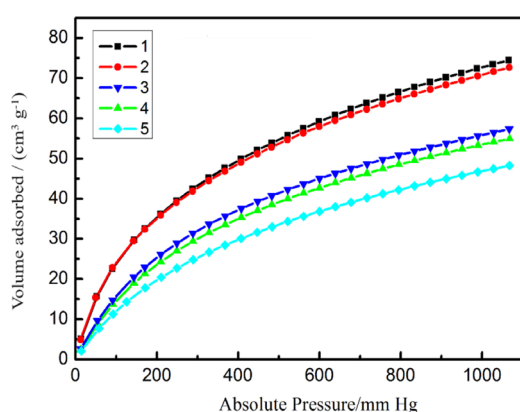
Figure 10. *CO₂ adsorption isotherm of the UiO-66-NH₂ at five cycles*

UiO-66-NDC, and UiO-66-BPDC) with different functionalized linkers and similar crystal structures. The CO_2 adsorption performances of these UiO-66-type MOFs were presented and discussed. UiO-66-NH₂ exhibited much higher CO_2 adsorption uptake (3.35 mmol g⁻¹) than other bulkier groups. The higher polarity of UiO-66-NO₂ led to its stronger interactions with polar functional groups, while UiO-66-2,5-(OH)₂ demonstrated a greater synergistic affinity to uptake CO_2. UiO-66-NDC and UiO-66-BPDC had lower BET surface areas, signifying their poor uptake of CO_2. In addition, multiple consecutive adsorption regeneration tests suggested that the CO_2 working capacity of UiO-66-NH₂ can be fully recovered after cyclic regeneration. UiO-66-type MOFs with different ligands were thus demonstrated as effective and stable adsorbents for CO_2 adsorption applications.

ACKNOWLEDGMENTS

REFERENCES

1. Gagliardi, L.; Yaghi, O. M.; *Chem. Mater.* **2023**, *35*, 5711. [Crossref]
2. Yang, X.; Li, Z.; Tang, S. K.; *Cryst. Growth Des.* **2021**, *21*, 6092. [Crossref]
3. Raganati, F.; Miccio, F.; Ammendola P.; *Energy Fuels* **2021**, *35*, 12845. [Crossref]
4. Seoane, B.; Coronas, J.; Gascon, I.; Benavides, M. E.; Karvan, O.; Caro, J.; Kapteijn, F.; Gascon, J.; *Chem. Soc. Rev.* **2015**, *44*, 2421. [Crossref]
5. Jia, B.; Bing, L.; Xu, B.; Sun, J.; Bai, S.; *Langmuir* **2022**, *38*, 14644. [Crossref]
6. Parsaei, M.; Akhbari, K.; White. J.; *Inorg. Chem.* **2022**, *61*, 3893. [Crossref]
7. Jasuja, H.; Zang, J.; Sholl, D. S.; Walton, K. S.; *J. Phys. Chem. C* **2012**, *116*, 23526. [Crossref]
8. Kim, S.; Yoon, T. U.; Oh, K. H.; Kwak, J.; Bae, Y. S.; Kim, M.; *Inorg. Chem.* **2020**, *59*, 18048. [Crossref]
9. Wang, D. C.; Xin, Y. Y.; Li, X. Q.; Ning, H. L.; Wang, Y. D.; Yao, D. D.; Zheng, Y. P.; Meng, Z. Y.; Yang, Z. Y.; Pan, Y. T.; Li, P. P.; Wang, H. N.; He, Z. J.; Fan, W. D.; *ACS Appl. Mater. Interfaces* **2021**, *13*, 2600. [Crossref]
10. Hack, J.; Maeda, N.; Meier, D. M.; *ACS Omega* **2022**, *7*, 39520. [Crossref]
11. Coelho, J. A.; Ribeiro, A. M.; Ferreira, P.; Lucena, S.; Rodrigues, A. E.; Azevedo, D.; *Ind. Eng. Chem. Res.* **2016**, *55*, 2134. [Crossref]
12. Wang, Y.; Wang, S. D.; Li, Z.; Sun, L. W.; Yang, X. Y.; Tang, S. K.; *Ind. Eng. Chem. Res.* **2021**, *60*, 771. [Crossref]
13. Yu, J. M.; Balbuena, P. B.; *ACS Sustainable Chem. Eng.* **2015**, *3*, 117. [Crossref]
14. Liang, Z. H.; Ou, Y. Y.; Sayed, E. M.; Su, K. Z.; Wang, W. J.; Yuan, D. Q.; *Inorg. Chem.* **2023**, *62*, 8309. [Crossref]
15. Ning, H. L.; Yang, Z. Y.; Yin, Z. Q.; Wang, D. C.; Meng, Z. Y.; Wang, C. G.; Zhang, Y. T.; Chen, Z. P.; *ACS Appl. Mater. Interfaces* **2021**, *13*, 17781. [Crossref]
16. Hernandez, A. F.; Impastato, R. K.; Hossain, M. I.; Rabideau, B. D.; Glover, T. G.; *Langmuir* **2021**, *37*, 10439. [Crossref]
17. Abramova, A.; Couzon, N.; Leloire, M.; Nerisson, P.; Cantrel, L.; Royer, S.; Loiseau, T.; Volkringer, C.; Dhainaut, J.; *ACS Appl. Mater. Interfaces* **2022**, *14*, 10669. [Crossref]
18. Ghosh, P.; Colon, Y. J.; Snurr, R. Q.; *Chem. Commun.* **2014**, *50*, 11329. [Crossref]
19. Chaemchuen, S.; Kabir, N. A.; Zhou, K.; Verpoort, F.; *Chem. Soc. Rev.* **2013**, *42*, 9304. [Crossref]
20. Li, Y. F.; Liu, Y.; Gao, W. Y.; Zhang, L. M.; Liu, W.; Lu, J. J.; Wang, Z.; Deng. Y. J.; *CrysEngComm* **2014**, *16*, 7037. [Crossref]
21. Biswas, S.; Zhang, J.; Li, Z. B.; Liu, Y. Y.; Grzywa, M.; Sun, L. X.; Volkmerc, D.; Voort, P.; *Dalton Trans.* **2013**, *42*, 4730. [Crossref]
22. Yang, Q. Y.; Wiersum, A. D.; Llewellyn, P. L.; Guillerm, V.; Serred, C.; Maurin, G.; *Chem. Commun.* **2011**, *47*, 9603. [Crossref]
23. Cmarik, G. E.; Kim, M.; Cohen, S. M.; Walton, K. S.; *Langmuir* **2012**, *28*, 15606. [Crossref]
24. Rada, Z. H.; Abid, H. R.; Shang, J.; Sun, H. Q.; He, Y. D.; Webley, P.; Liu, S. M.; Wang, S. B.; *Ind. Eng. Chem. Res.* **2016**, *55*, 7924. [Crossref]
25. Yang, Z. Q.; Ying, Y. P.; Pu, Y. C.; Wang, D. C.; Yang, H.; Zhao, D.; *Ind. Eng. Chem. Res.* **2022**, *61*, 7626. [Crossref]
26. Kandiah, M.; Nilsen, M. H.; Usseglio, S.; Jakobsen, S.; Olsbye, U.; Tilset, M.; Larabi, C.; Quadrelli, E. A.; Bonino, F.; Lillerud, K. P.; *Chem. Mater.* **2010**, *22*, 6632. [Crossref]
27. Valenzano, L.; Civalleri, B.; Chavan, S.; Bordiga, S.; Nilsen, M. H.; Jakobsen, S.; Lillerud, K. P.; Lamberti, C.; *Chem. Mater.* **2011**, *23*, 1700. [Crossref]
28. Saito, M.; Toyao, T.; Ueda, K.; Kamegawa, T.; Horiuchi, Y.; Matsuoka, M.; *Dalton Trans.* **2013**, *42*, 9444. [Crossref]

29. Yoo, D. K.; Woo, H. C.; Jhung, S. H.; *ACS Appl. Mater. Interfaces* **2020**, *12*, 34423. [Crossref]

30. Hu, Z. G.; Peng, Y. W.; Kang, Z. X.; Qian, Y. H.; Zhao, D.; *Inorg. Chem.* **2015**, *54*, 4862. [Crossref]

31. Rada, Z. H.; Abid, H. R.; Sun, H. Q.; Wang, S. B.; *J. Chem. Eng. Data* **2015**, *60*, 2152. [Crossref]

32. Anjum, M. W.; Vermoortele, F.; Khan, A. L.; Bueken, B.; Vos, D. E.; Vankelecom, I. J.; *ACS Appl. Mater. Interfaces* **2015**, *7*, 25193. [Crossref]

33. Wu, H.; Chua, Y. S.; Krungleviciute, V.; Tyagi, M.; Chen, P.; Yildirim, T.; Zou, W.; *J. Am. Chem. Soc.* **2013**, *135*, 10525. [Crossref]

34. Ragon, F.; Campo, B.; Yang, Q. Y.; Martineau, C.; Wiersum, A. D.; Lago, A.; Guillerm, V.; Hemsley, C.; Eubank, J. F.; Vishnuvarthan, M.; Taulelle, F.; Horcajada, P.; Vimont, A.; Llewellyn, P. L.; Daturi, M.; Vinot, S. D.; Maurin, G.; Serre, C.; Devic, T.; Clet, G.; *J. Mater. Chem. A* **2015**, *3*, 3294. [Crossref]

35. Shearer, G. C.; Chavan, S.; Ethiraj, J.; Vitillo, J. G.; Svelle, S.; Olsbye, U.; Lamberti, C.; Bordiga, S.; Lillerud, K. P.; *Chem. Mater.* **2014**, *26*, 4068. [Crossref]

36. Jasuja, H.; Walton, K. S.; *J. Phys. Chem. C* **2013**, *117*, 7062. [Crossref]

37. Katz, M. J.; Brown, Z. J.; Colon, Y. J.; Siu, P. W.; Scheidt, K. A.; Snurr, R. Q.; Hupp, J. T.; Farha, O. K.; *Chem. Commun.* **2013**, *49*, 9449. [Crossref]

38. Silva, P.; Vilela, S. M.; Tome, J. P.; Paz, F. A.; *Chem. Soc. Rev.* **2015**, *44*, 6774. [Crossref]

39. Dong, Z.; Hu, W. D.; Liu, H. J.; Yang, Z. Z.; Moitra, D.; Jiang, D. E.; Dai, S.; Hu, J. Z.; Wu, D.; Lin, H. F.; *ACS Appl. Nano Mater.* **2023**, *6*, 12159. [Crossref]

40. Magnin, Y.; Dirand, E.; Orsikowsky, A.; Plainchault, M.; Pugnet, V.; Cordier, P.; Llewellyn, P. L.; *J. Phys. Chem. C* **2022**, *126*, 3211. [Crossref]

41. Lv, G. R.; Liu, J. M.; Xiong, Z. H.; Zhang, Z. H.; Guan, Z. Y.; *J. Chem. Eng. Data* **2016**, *61*, 3868. [Crossref]

42. Zhu, X. Y.; Gu, J. L.; Wang, Y.; Li, B.; Li, Y. S.; Zhao, W. R.; Shi, J. J.; *Chem. Commun.* **2014**, *50*, 8779. [Crossref]

43. Han, Y. T.; Liu, K. M.; Li, Y.; Zuo, Y.; Wei, Y. X.; Xu, S. T.; Zhang, G. L.; Song, C. S.; Zhang, Z. C.; Guo, X. W.; *CrystEngComm* **2015**, *17*, 6434. [Crossref]

44. Hu, Z. G.; Nalaparaju, A.; Peng, Y. W.; Jiang, J. W.; Zhao, D.; *Inorg. Chem.* **2016**, *55*, 1134. [Crossref]

45. Hendrickx, K.; Vanpoucke, D.; Leus, K.; Lejaeghere, K.; Deyne, A.; Speybroeck, V. V.; Voort, P. V.; Hemelsoet, K.; *Inorg. Chem.* **2015**, *54*, 10701. [Crossref]

46. Yang, E.; Li, H. Y.; Wang, F.; Yang, H.; Zhang, J.; *CrystEngComm* **2013**, *15*, 658. [Crossref]

47. Luo, L. M.; Xu, C. Y.; Shi, W. L.; Liu, Q.; Ou-Yang, Y. Y.; Qian, J.; Wang, Y. Q.; Li, Q.; *J. Phys. Chem. Lett.* **2023**, *14*, 8437. [Crossref]

48. Hasell, T.; Armstrong, J. A.; Jelfs, K. E.; Tay, F. H.; Thomas, K. M.; Kazarian, S. G.; Cooper, A. I.; *Chem. Commun.* **2013**, *49*, 9410. [Crossref]

49. Yang, Q. Y.; Wiersum, A. D.; Jobic, H.; Guillerm, V.; Serre, C.; Llewellyn, P. L.; Maurin, G.; *J. Phys. Chem. C* **2011**, *115*, 13768. [Crossref]

50. Xian, S. K.; Wu, Y.; Wu, J. L.; Wang, X.; Xiao, J.; *Ind. Eng. Chem. Res.* **2015**, *54*, 11151. [Crossref]